Aspects of Steady State Operation of the Wendelstein 7-X Stellarator

J Geiger[1], R C Wolf[1], C Beidler[1], A Cardella[1], E Chlechowitz[1], V Erckmann[1], G Gantenbein[2], D Hathiramani[1], M Hirsch[1], W Kasparek[3], J Kißlinger[1], R König[1], P Kornejew[1], H P Laqua[1], C Lechte[3], J Lore[4], A Lumsdaine[4], H Maaßberg[1], N B Marushchenko[1], G Michel[1], M Otte[1], A Peacock[1], T Sunn Pedersen[1], M Thumm[2], Y Turkin[1], A Werner[1], D Zhang[1], and the W7-X Team

[1]Max-Planck-Institute for Plasma Physics, EURATOM Association, Garching and Greifswald, Germany

[2]Karlsruhe Institute for Technology, IHM, EURATOM Association, Karlsruhe, Germany

[3]Institute for Plasma Research, University of Stuttgart, Stuttgart, Germany

[4]Oak Ridge National Laboratory, Oak Ridge, TN, USA

E-mail: robert.wolf@ipp.mpg.de

Abstract. The objective of Wendelstein 7-X is to demonstrate steady state operation at β-values of up to 5%, at ion temperatures of several keV and plasma densities of up to 2×10^{20} m^{-3}. The second operational phase foresees a fully steady state high heat flux divertor. Preparations are underway to cope with residual bootstrap currents, either by electron cyclotron current drive or by high heat flux protection elements. The main steady state heating system is an electron cyclotron resonance heating facility. Various technical improvements of the gyrotrons have been implemented recently. They enable a reliable operation at the 1 MW power level. Some of the technical issues preparing plasma diagnostics for steady state operation are exemplified. This includes the protection against non-absorbed microwave radiation.

1. Introduction

Wendelstein 7-X (W7-X) is a drift-optimized stellarator which has been designed to demonstrate the reactor capability of the stellarator concept (Beidler *et al.* 1990, Grieger *et al.* 1992, Wolf *et al.* 2008). This includes improved neoclassical confinement of both thermal plasma and fast ions, sufficiently high stability and equilibrium limits and a feasible exhaust concept. Taking these elements together the main objective is to achieve steady state operation at high normalized plasma pressure with values of the volume averaged β of about 5%, ion temperatures of several keV and plasma densities of 10^{20} m^{-3} and higher. Plasma exhaust relies on a resonant island divertor (Renner *et al.* 1998) which requires, as far as possible, a magnetic equilibrium configuration which is not influenced by the plasma β. This means that Shafranov shift and bootstrap current have to remain small. With the 5-fold periodicity of the machine, a low-shear rotational transform profile with a boundary value of 5/5 (toroidal to poloidal mode number) generates the large magnetic islands for the island divertor, while avoiding major resonances in the plasma. Flexibility in the coil system also allows boundary ι values of 5/6 and 5/4 with corresponding island chains.

The magnetic field configurations are realized by 70 superconducting coils. 50 non-planar modular coils provide the basic rotational transform. 20 planar coils allow to vary the rotational transform and to adjust the radial position of the plasma. Sweeping of the divertor strike lines is facilitated by 10 normally conducting divertor coils. In addition, five normally conducting trim coils are introduced outside the cryostat vessel for plasma edge control and error field correction. The achievable magnetic field is 3 T. A major radius of R = 5.5 m and an average minor radius of $\langle a \rangle$ = 0.55 m correspond to a plasma volume of about 30 m^3.

The completion of the assembly of Wendelstein 7-X is foreseen in 2014. During the initial phase of operation, starting after the commissioning phase in 2015, limitations of the cooling of in-vessel components will limit the pulse length (Bosch *et al.* 2010). At 10 MW heating power pulse durations of about 10 s are expected. Reducing this to 1 MW, the pulse lengths can be extended to just one minute. During a two years completion phase between 2017 and 2019 the full steady state capability of Wendelstein 7-X will be implemented. This in particular involves the installation of an actively cooled high heat flux (HHF) divertor designed for heat fluxes of up to 10 MW/m^2. Although the optimization of W7-X includes the minimization of the bootstrap current, the degree of the minimization is dependent on the magnetic configuration. Since W7-X has no ohmic transformer to control a toroidal net-current, plasma scenarios in magnetic configurations with less minimized bootstrap current lead to changes in the plasma boundary topology on the L/R time which is of the order of 30 s. To protect sensitive areas of the HHF-divertor which might see unwanted heat loads either the toroidal net-current needs to be limited or additional passive protection measures are required. Possible methods are a proper choice of the magnetic configuration with minimum bootstrap current, current drive by electron cyclotron waves to compensate for the effect of a finite bootstrap current or specially designed protection tiles, which intersect those open field lines in the scrape-off-layer otherwise carrying heat to areas not designed for high heat fluxes.

Also heating systems, plasma fuelling, plasma diagnostics, data acquisition and experiment control have to be designed for steady state operation. The main heating system consists of ten continuous-wave gyrotrons with output powers between 700 kW and 1 MW, operating at 140 GHz for electron cyclotron resonance heating at 2.5 T. The heating by the injection of neutral hydrogen or deuterium atoms is restricted to 10 s pulses. The development of a design for an ion cyclotron resonance heating system has just started.

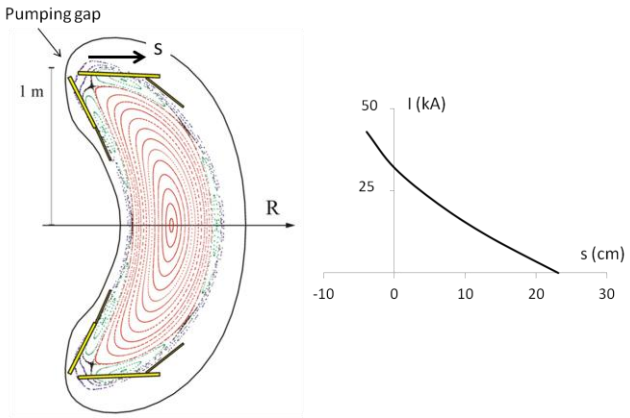

Figure 1: On the left, a Poincaré plot of the magnetic field lines in the poloidal plane (bean shaped cross-section) is shown, indicating flux surfaces and regions of open magnetic field lines intersecting the divertor target plates (vacuum magnetic field of the standard configuration at $\iota = 1$). The plot on the right shows the dependence between the strike point position, s, and the plasma current, I. At s = 0 the strike point is located at the edge of the target plate. Negative s means that the strike point is inside the pumping gap where large heat fluxes cannot be tolerated.

For understanding the requirements of steady state operation, the interaction of the plasma with the plasma facing components and the time scales governing plasma confinement and stability have to be considered. The actively cooled first wall will reach thermal equilibrium after several seconds or remote parts receiving only small heat fluxes after minutes. Similarly, the equilibrium of the gas inventory stored in the wall will be reached after a few seconds, not accounting for the build-up of co-deposited layers which at least for carbon form a constantly increasing reservoir of hydrocarbon compounds (Tsitrone *et al.* 2009). Finally, net erosion and neutron damage limit the life time of

plasma facing components. The latter two effects, however, are not relevant for W7-X, although long pulse operation will give insight into the erosion processes on much shorter time scales compared to experiments with plasma pulses of only a few seconds.

This paper is structured as follows: First, divertor operation and the handling of residual amounts of bootstrap current are described. It will be explained why even for transient plasma states basically steady state solutions for in-vessel components become necessary. The second part of the paper focuses on the progress made with the electron cyclotron resonance heating (ECRH) system. Finally, steady state diagnostic requirements are discussed including protection measures against stray radiation from non-absorbed microwaves.

2. Plasma operation and divertor control

The W7-X divertor consists of ten modules whose target plates intersect the magnetic islands of the plasma boundary (Renner *et al.* 1998). While in the poloidal plane the arrangement is similar to a poloidal divertor of a tokamak (figure **1**), along the helical coordinate heat loads and divertor are discontinuous. The exact position of the strike points is determined by the plasma equilibrium. Since the magnetic islands are the result of the resonance condition of $\iota = 1$ at the plasma boundary, the divertor magnetic field topology sensitively depends on plasma currents such as the bootstrap current (Geiger *et al.* (1) 2010 and Geiger *et al.* 2011). The so-called standard configuration has a very good confinement but is less optimized for minimum bootstrap current which can reach levels inhibiting proper divertor operation (Geiger *et al.* (2) 2010). The name "standard configuration" reflects the fact that only the modular coil system (same current in all 5 coil types) is used but not the planar coils. In the standard configuration at 5 MW of ECRH power and low density ($5{\cdot}10^{19}$m^{-3}) bootstrap currents of up to 50 kA are expected reducing to 10 kA at high density ($2{\cdot}10^{20}$m^{-3}). The change of the plasma boundary during the evolution of the plasma current on the L/R-time results in a movement of the strike points with corresponding heat loads to sensitive areas such as the edges of the divertor tiles or the pumping gap between target plates. The movement of the strike points is illustrated in figure **1**.

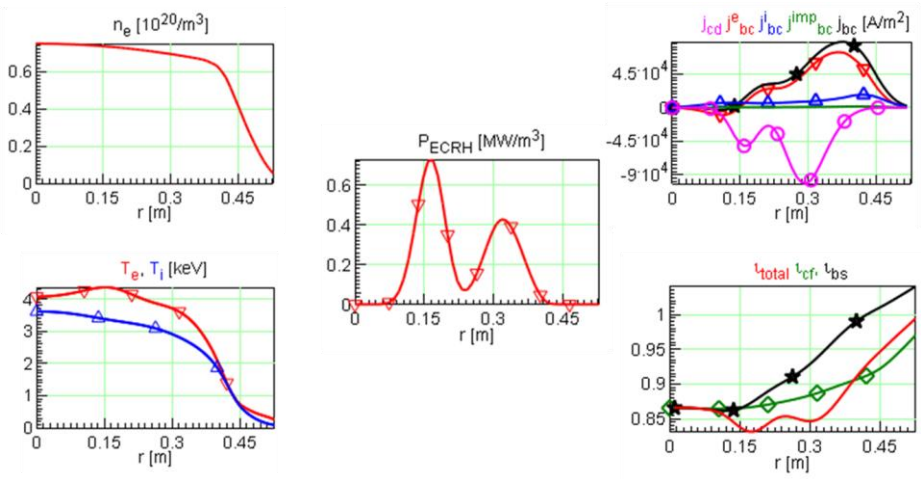

Figure 2: Simulation of the compensation of the bootstrap current by ECCD. From left to right: Underlying temperature (ions and electrons) and density profiles, radial distribution of power density of the electron cyclotron resonance waves, and components of the current density and ι-profiles. Shown are the contributions from current drive (cd) and bootstrap current (bc with contributions from electron, ions and impurities). The total ι-profile with bootstrap current and current drive is compared to the ι-profile with bootstrap current alone (bs) and to the current free case (cf).

Negative values of the s-coordinate along the tile surface means that the heat flux is entering the pumping gap; s=0 is located at the edge of the divertor tiles which by design can only accept a reduced heat flux between 2 to 5 MW/m^2 (Peacock *et al.* 2011).

Here, two possibilities how to deal with a finite bootstrap current are discussed. First, EC-current drive is used to compensate the bootstrap current for toroidal net-current free operation. Second, for the case of non-compensated finite bootstrap current tiles are introduced as passive protection measure to scrape-off the flux bundles carrying the heat load to sensitive areas while the magnetic configuration changes during the evolution of the plasma current.

2.1. Control of the rotational transform by electron cyclotron resonance current drive

Electron cyclotron current drive (ECCD) for bootstrap current compensation in a low shear stellarator needs to consider different aspects: (i) the bootstrap current is driven by the gradients of temperature and density while the heating and thus the current drive is at the maximum of the electron temperature which makes ECCD not capable to perfectly compensate the bootstrap current density locally; (ii) ECRH is a local heating scheme and thus ECCD produces large local current densities resulting in strong deviations of the ι-profile contrary to the idea of a low shear device; (iii) the ECCD-efficiency depends on the heating scheme. For X2-mode (densities up to 10^{20} m^{-3}) ECCD-efficiency is good, but for O2-mode heating required for high density operation (up to $2.4\cdot10^{20}$ m^{-3}) it is poor. Figure **2** shows a simulation at medium density ($n_e=7\cdot10^{19}$m^{-3}, 5MW 140GHz X2-mode heating) in which a compensation of the bootstrap current is attempted locally as best as possible with ECCD (Turkin *et al.* 2006). For this purpose P_{ECRH} of 5MW is launched in two beams with different toroidal launching angles (current drive) and different vertical off-set to get different radial deposition zones. The inner beam (2MW) is used mainly for heating (small ECCD-contribution), while the outer beam (3MW) carries the main part of the ECCD. However this technique also broadens the overall heating deposition profile. As a result of the off-axis current drive the current densities roughly match and the

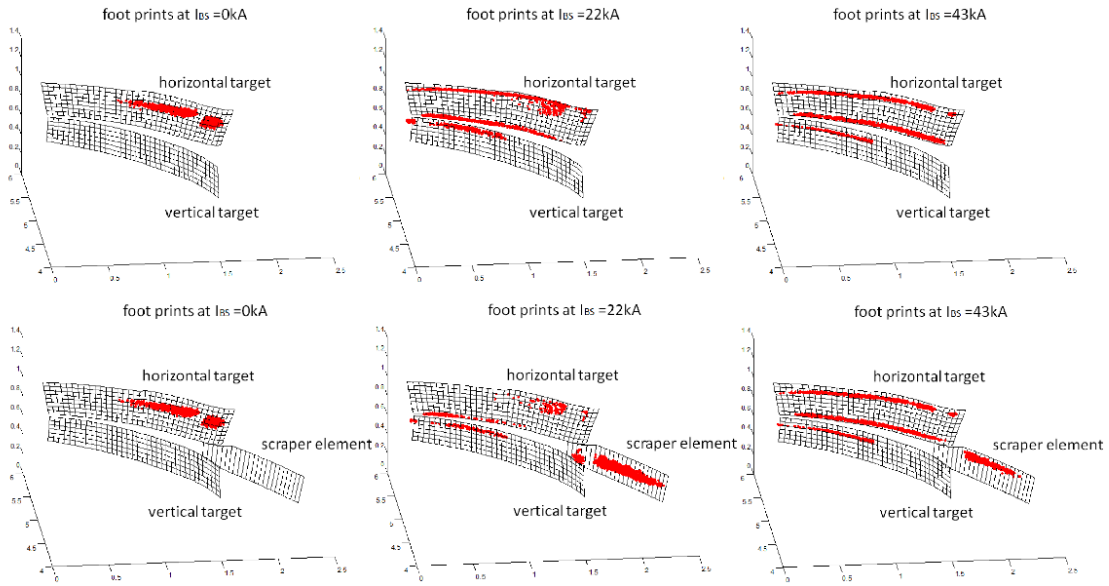

Figure 3: Working principle of the scraper element for a scenario with a bootstrap current of 43kA. The top/bottom row shows the strike point distribution (Poincaré plots) on the divertor targets without/with the scraper element. The plots from left to right show the evolution of the toroidal net-current. Left: limiter-configuration with bootstrap current fully shielded by self-inductance of the plasma; middle: half of the bootstrap current is shielded; right: shielding current has decayed, magnetic configuration with full bootstrap current forms appropriate separatrix with islands for proper divertor operation. The scraper element protects the critical areas at the pumping gap during the evolution (middle) of the magnetic configuration from a non-critical limiter configuration (left) to the final desired island divertor configuration (right).

resulting ι-profile agrees fairly well with the current free case. In contrast, the ι-profile without bootstrap current compensation shows a deviation of the edge rotational transform of more than 5% with the result that the boundary islands would have moved further in the confinement region.

At densities above 10^{20} m^{-3}, O2-mode heating will be applied, but this heating scheme has insufficient ECCD-efficiency to compensate the predicted bootstrap currents (Geiger *et al.* (2) 2010). For experiments in configurations which lack the full minimization of the bootstrap current a different scheme needs to be considered. The rotational transform of the magnetic vacuum configuration is adjusted such that with the predicted bootstrap current a boundary configuration with the required islands is created to allow a proper island divertor operation. For example, with a bootstrap current predicted to increase the boundary ι -value, the discharge starts in a configuration with a lower boundary value of ι corresponding to a limiter configuration. Initially, the bootstrap-current is shielded by the self-inductance of the plasma, but this part decays in time and the net-current evolves on the L/R-time (no ohmic transformer!) so that the boundary configuration gradually changes until finally the proper island divertor configuration is formed. However, the slowly changing magnetic boundary configuration leads to moving heat loads which are critical at the edges of the divertor targets and the pumping gap.

2.2. Scraper element for divertor protection

In order to protect the sensitive divertor areas protection tiles have to be introduced. The working principle of this so-called scraper element (Peacock *et al.* 2011) is illustrated in figure 3. A high-density plasma ($1.5\times10^{20}m^{-3}$) is heated with 7MW ECRH (140GHz, O2-mode) and the predicted bootstrap current is 43kA. The vacuum configuration has been adjusted to a lower rotational transform value such that the bootstrap current provides the missing rotational transform to generate the island structure for the island divertor. Figure 3 shows three stages in the evolution of the heat flux patterns in the previously described evolution of the toroidal net-current on the L/R-time and compares the patterns with (bottom row) and without (top row) scraper element. In the initial configuration – a limiter configuration with bootstrap current shielded by self-inductance, thus vanishing plasma current – the scraper element sees no heat flux and the power deposition on the divertor tiles does not differ for the two cases (top/bottom). The limiter situation of the boundary configuration is reflected in a concentration of the flux pattern along the helical direction of the divertor tiles. The critical situation appears during the evolution phase of the plasma current – the middle column of figure 3 shows the plasma current evolved half-way, i.e. 22kA – while the initial limiter configuration and the final island divertor configuration are uncritical. Without scraper element heat flux reaches the tile edges (22 kA case, top row of figure **3**) which are designed for only 2 and 5 MW/m^2 (Peacock *et al.* 2011). The scraper element prevents heat flux reaching these sensitive areas (22 kA case, bottom row of figure **3**). In the final state, when the current evolution is completed, the edge-ι meets the resonance condition and the scraper element receives only little heat loads (43 kA case, bottom row of figure **3**). The estimated maximum heat load to the scraper element is 12 MW/m^2 (Peacock *et al.* 2011). Due to the long L/R-time the requirement is to remove such amounts of heat for 30 s or more and thus needs an actively cooled structure. The solution proposed for this application is based on CFC-monoblock design similar to plasma facing components qualified for ITER (Riccardi *et al.* 2011).

3. Steady state heating

The steady state heating system for W7-X is an ECRH facility prepared for ten gyrotrons. The frequency of the gyrotrons is 140 GHz, corresponding to the 2nd harmonic gyro-frequency of the electrons at 2.5 T (Erckmann *et al.* 2007). Each gyrotron is designed for a steady state output power of 1 MW. The specified acceptance criterion is a minimum of 900 kW over 30 minutes. At present five

gyrotrons are ready for operation. At least three further gyrotrons will be manufactured until the beginning of the W7-X operation, assuming a total output power of about 7.5 MW. Although the gyrotron prototype developments were successful, problems with meeting the specifications led to several modifications which had to be implemented during series production (Gantenbein *et al.* 2010). This included a new beam tunnel design to avoid spurious oscillations before the electron beam reaches the cavity and an improved power handling in the collector using a rotating transverse magnetic field (Braune *et al.* 2009). Since the rotating transverse magnetic field removes the peak temperatures in the turning points of the electron beam inside the single-stage depressed collector, the overall power to the collector can be increased significantly. The effect on the output power of the gyrotron is illustrated in figure **4**. As a consequence 1 MW output power has been achieved despite efficiencies of ~40%.

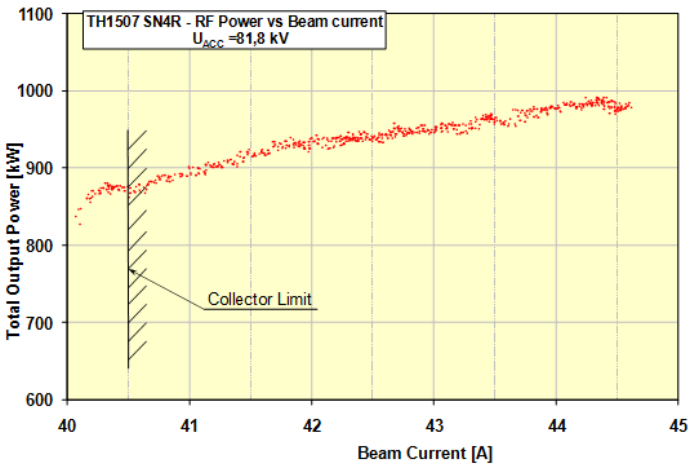

Figure 4: Dependence of total power output on electron beam current for a gyrotron with improved collector sweeping. The previous collector limit without the transverse rotating magnetic field would have clamped the power below the specified 900 kW. With the improvement 1 WM has been achieved.

Basically all the transmission components are fabricated and tested. The power from the gyrotrons is collected and relayed through air to W7-X by mirrors (Erckmann *et al.* 2007). This quasi-optical transmission line has a very high efficiency limiting the losses to about 7%. For the coupling into the plasma four launchers, each equipped with three front steering mirrors, are available permitting for each gyrotron to individually change the poloidal and toroidal launch angles. At a given resonance this means that for each gyrotron the vertical position of the deposition (in the poloidal plane) can be selected, and modifying the toroidal angle also the amount of current drive.

For plasma start-up and at low plasma densities 2nd harmonic X-mode (X2) heating will be applied. Above the cut-off density of about 1.2×10^{20} m^{-3} the X2-mode can be changed to the 2nd harmonic O-mode by modifying the polarization of the microwave radiation. Especially during this transition, but also during O2-heating the non-absorbed power increases, requiring multi-pass absorption. Although this is foreseen, using mirrors inside the plasma vessel, it is assumed that a significant level of stray radiation will remain. Due to multiple reflections in the plasma chamber the stray radiation becomes nearly isotropic behaving like a gas of photons. The local level of stray radiation depends on the source strength, the plasma absorption which depending on the heating scenario is a function of electron density and temperature, and the absorption by in-vessel components. Generally, the expected stray radiation level decreases with increasing distance from the ECRH launchers (Laqua *et al.* 2001, Hartfuss *et al.* 2003). A factor of ten is expected in W7-X. Therefore all in-vessel components, including diagnostics, cabling, etc., have to be qualified and if necessary protected to withstand up to

50 kW/m^2 of continuous microwave power flux, corresponding to a total non-absorbed microwave power of up to 1 MW (Hirsch *et al.* 2010). Critical components are tested inside the microwave stray radiation launch (MISTRAL) facility which is a large vacuum chamber made of aluminum for a high reflection coefficient and connected to one of the gyrotrons.

4. Steady state diagnostics

Steady state diagnostics have to fulfil many requirements. A comprehensive overview is given in Hartfuss *et al.* 2006. The requirements range from steady state detection and data acquisition to protection against even low radiation and particle fluxes from the plasma, often requiring elaborate cooling techniques (König *et al.* 2010). In addition, a steady state plasma experiment asks for diagnostics which are capable to continuously monitor the plasma facing components. As a consequence both data rates and data amounts increase significantly. For W7-X about 30 Gbyte/s are expected corresponding to 50 Tbyte for a 30 minutes plasma.

One example development for the application on W7-X is an interferometer to measure the line integrated density. The test measurements on the TEXTOR tokamak are described in Dreier *et al.* 2011. The operational requirements of an interferometer combine very different time scales. On the one hand, it has to be insensitive against vibrations and capable of following fast density changes. On the other hand, the density measurement has to be insensitive against temperature changes and generally requires long-term stability. The chosen technique is a so-called dispersion interferometer, which uses a frequency doubler so that two phase coupled laser beams (1st and 2nd harmonic) travel through the plasma. Then also the frequency of the 1st harmonic beam is doubled. The superposition of the two harmonics significantly reduces the sensitivity of the instrument to vibrations as no separate reference arm is needed and both signals stem from identical geometrical path lengths. Another advantage, using the superposition of two harmonics of the same laser, is that the measured phase shift is directly proportional to the line integrated density. Phase shifts ~2π allow the reconstruction of the signal by simple interpolation should this be lost during operation.

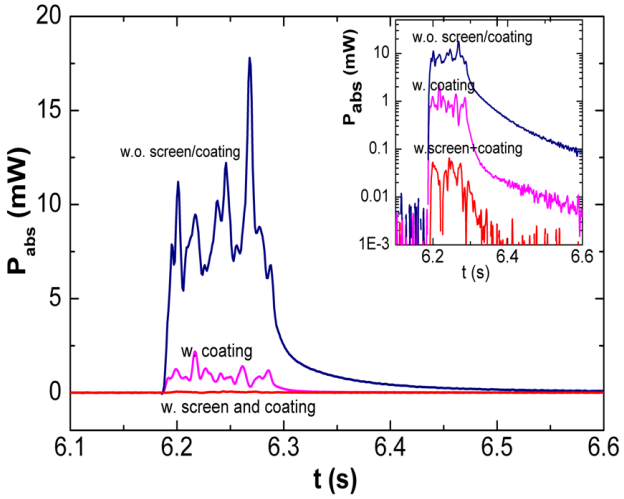

Figure 5: The bolometer is exposed to microwave stray radiation only. Compared are the absorbed power without any protection measures, with a microwave absorbing coating inside the detector housing and, in addition, with a metal mesh in front of the bolometer foils. The first measure (with coating) reduces the signal by a factor of 10, the second measure (with screen and coating) by an additional factor of 30.

Standard analogue integrators used for instance together with magnetic probes do not work under long pulse conditions. For the application on W7-X a digital integrator has been developed which

compensates the amplifier drifts and has an output stage which is not limited by the dynamic range (Werner 2006). In recent experiments on the stellarator experiment WEGA plasma currents of 1 A (measured with a Rogowski coil) and plasma energies of 1 J (measured with a diamagnetic loop) have been resolved, confirming the high sensitivity, the low integrator drift ($\sim 10^{-4}$) and the high relative resolution ($\sim 10^{-5}$).

The aforementioned stray radiation can also influence measurements directly. The principle of a resistive bolometer makes it sensitive to microwave radiation. Therefore, a method had to be found to minimize the impact of stray radiation, while maintaining its sensitivity to plasma radiation. The W7-X bolometer foils are contained in a closed detector housing with a pin hole basically forming a pinhole camera imaging the plasma on an array of radiation sensitive bolometer foils. In order to reduce the sensitivity to stray radiation the bolometer foils are covered by a metal mesh and the inside of the detector head is coated with a microwave absorbing material (a mixture of aluminium oxide and titanium oxide, for details see Zhang *et al.* 2010). The coating reduces the stray radiation level inside the bolometer head and the metal mesh screens the detectors from the remaining radiation. Together the two measures reduce the stray radiation signal by a factor of 300 (figure **5**).

5. Summary and conclusions

Wendelstein 7-X is designed for 30 minutes plasmas at heating powers of 10 MW, essentially covering all time scales relevant for steady state operation. This requires actively cooled plasma facing components, heating systems and diagnostics developed for steady state operation. An analysis of the expected plasma scenarios shows that technical or physics solutions have to be prepared to allow a safe operation of the actively cooled high heat flux divertor. Plasma heating will be provided by continuous-wave gyrotrons delivering up to 1 MW each. The realization of such high power levels required modifications of the design even during the manufacturing process, showing the technical difficulties handling high power levels under steady state conditions. When going from short to long pulse experiments also diagnostic techniques require dedicated design adaptations. This comprises both the measurement requirements and the protection against radiation and particle fluxes, increasing development, design and manufacturing efforts significantly.

References

Beidler C D, Grieger G, Herrnegger F, Harmeyer E, Kisslinger J, Lotz W et al. 1990 Physics and engineering design for Wendelstein VII-X *Fusion Techn.* **17** 148 – 168

Braune H. et al. 2009 Transverse field collector sweeping for the W7-X gyrotrons–modulation techniques *Proc. 34th IRMMW-THz* Busan, Korea, http://ieeexplore.ieee.org/stamp/stamp.jsp?arnumber=05325739

Bosch H-S, Dinklage A, Klinger T, Wolf R and the Wendelstein 7-X Team 2010 Physics Programme for Initial Operation of Wendelstein 7-X *Contrib. Plasma Phys.* **50** 687 – 694

Dreier H et al. 2011 First results from the modular multi-channel dispersion interferometer at the TEXTOR tokamak *Rev. Sci. Instrum.* **82** 063509

Erckmann V et al. 2007 Electron Cyclotron Heating for W7-X: Physics and Technology *Fusion Science and Technology* **52** 291

Gantenbein G et al. 2010 140 GHz, 1 MW CW Gyrotron Development for Fusion Applications – Progress and Recent Results *J. Infrared Milli TeraHz Waves* **32** 320 – 328

Geiger J *et al.* (1) 2010 Effects of Net Currents on the Magnetic Configuration of W7-X *Contrib. Plasma Phys.* **50** 770 – 774

Geiger J *et al.* (2) 2010 Physics Modeling for Steady-State Experiments at Wendelstein 7-X, *23rd IAEA Fusion Energy Conference 11-16 Oct. 2010, Daejon, Rep. of Korea*, http://www-pub.iaea.org/MTCD/Meeting/PDFplus/2010/cn180_papers/thc_p2-02.pdf

Geiger J *et al.* 2011 Erratum: Effects of Net Currents on the Magnetic Configuration of W7-X *Contrib. Plasma Phys.* **51** 99

Grieger G, Lotz W, Merkel P, Nührenberg J, Sapper J, Strumberger E et al. 1992 Physics optimization of stellarators *Phys. Fluids* B4 2081 – 2091

Hartfuss H-J, Erckmann V, Hirsch M, Laqua H 2003 Problems with ECRH stray radiation in Wendelstein 7-X *30th EPS Conference on Contr. Fusion and Plasma Phys., St. Petersburg, 7-11 July* ECA Vol. **27A**, O-3.2C, http://epsppd.epfl.ch/StPetersburg/PDF/O3_002C.PDF

Hartfuss H-J, König R, Werner A 2006 Diagnostics for steady state plasmas *Plasma Phys. Control. Fusion* **48** R83 – R150

Hirsch M et al. 2010 Qualifying Plasma Diagnostics for a High-Power Microwave Background of ECR-Heated Discharges *Proceedings of the International Conference on Plasma Diagnostics* April 12-16 Pont-à-Mousson, France, AIP conference proceedings

König R et al. 2010 Diagnostics design for steady-state operation of the Wendelstein 7-X stellarator *Rev. Sci. Instrum.* **81** 10E133

Laqua H P et al. 2011 Distribution of the ECRH stray radiation in fusion devices *In Proceedings of the 28th EPS Conf. Control. Fusion and Plasma Phys.,Funchal* (Eds.) C. Silva, C. Varandas, D. Campbell, ECA 25A, European Physical Society, Geneva 2001, 1277-1280. http://www.cfn.ist.utl.pt/EPS2001/fin/pdf/P3.099.pdf

Peacock A *et al.* 2011 A proposed scraper element to protect the end of the W7-X divertor target elements, *IEEE/NPSS 24th Symposium on Fusion Engineering (SOFE)*(Chicago, Illinois), 1 - 5

Renner H *et al.* 1998 Divertor Development for Wendelstein 7-X *J. Plasma Fusion Res. Series* **1** 743-147

Riccardi B et al. 2011 Preliminary results of the experimental study of PFCs exposure to ELM-like transient loads followed by high heat flux thermal fatigue *Fus. Eng. Des.* **86** 1665-1668

Tsitrone E et al. 2009 Deuterium inventory in Tore Supra: reconciling particle balance and post-mortem analysis *Nucl. Fusion* **49** 075011

Turkin Yu. *et al.* 2006 Current Control by ECCD for W7-X *Fusion Science and Technology*, **50**, 387 - 394

Werner A 2006 W7-X magnetic diagnostics: Performance of the digital integrator *Rev. Sci. Intrum.* **77** 10E307

Wolf R C and the Wendelstein 7-X Team 2008 A stellarator reactor based on the optimization criteria of Wendelstein 7-X *Fusion Eng. and Design* **83** 990 – 996

Zhang D *et al.* 2010 Design criteria of the bolometer diagnostic for steady-state operation of the W7-X stellarator *Rev. Sci. Instrum.* **81** 10E134